Bioresponsive nanotherapy for preventing dental caries by inhibiting multispecies cariogenic biofilms

Danfeng Liu [a,1], Xianbin Ma [b,1], Yaoting Ji [a], Rourong Chen [a], Shuhui Zhou [a], Hantao Yao [a], Zichen Zhang [a], Mengjie Ye [b], Zhigang Xu [b,**], Minquan Du [a,*]

[a] The State Key Laboratory Breeding Base of Basic Science of Stomatology (Hubei-MOST) and Key Laboratory of Oral Biomedicine Ministry of Education, School and Hospital of Stomatology, Wuhan University, Wuhan, 430079, PR China
[b] School of Materials and Energy & Chongqing Engineering Research Center for MicroNano Biomedical Materials and Devices, Southwest University, Chongqing, 400715, PR China

ABSTRACT

Early childhood caries (ECC) is a public healthcare concern that greatly reduces the quality of life of young children. As a leading factor of ECC, cariogenic biofilms are composed of acidogenic/aciduric pathogens and extracellular polysaccharides (EPSs), creating an acidic and protected microenvironment. Antimicrobial photodynamic therapy (aPDT) is a noninvasive, painless, and efficient therapeutic approach that is suitable for treating ECC. However, due to the hyperfine structure of cariogenic biofilms, most photosensitizers (PSs) could not access and penetrate deeply in biofilms, which dramatically hamper their efficiency in the clinic. Herein, bioresponsive nanoparticle loaded with chlorin e6 (MPP-Ce6) is developed, which largely increases the penetration depth (by over 75%) and retention (by over 100%) of PS in the biofilm compared with free Ce6. Furthermore, MPP-Ce6-mediated aPDT not only kills the bacteria in preformed biofilms but also inhibits multispecies biofilm formation. A rampant caries model is established to mimic ECC *in vivo*, where the population of cariogenic bacteria is decreased to 10% after MPP-Ce6-mediated aPDT. Importantly, the number and severity of carious lesions are efficiently reduced *via* Keyes' scoring and micro-CT analysis. This simple but effective strategy can serve as a promising approach for daily oral hygiene in preventing ECC.

1. Introduction

Dental caries remains a global public health problem, with more than 2.4 billion individuals affected worldwide [1]. Early childhood caries (ECC) is a more aggressive and rapidly developed caries that affects more than 90% of 3- to 5-year-old young children [2]. Dental caries has multifactorial etiologies, including host factors, bacteria, substrate, and time [3], where cariogenic microbiota-mediated biofilms, also known as dental plaques, play a decisive role in the development of dental caries. During the formation of dental plaque, "pioneer" species, such as *Streptococcus sanguinis* (*S. sanguinis*), adhere to the tooth surfaces firstly. Acidogenic/aciduric species, such as *Streptococcus mutans* (*S. mutans*) and *Streptococcus sobrinus* (*S. sobrinus*), aggregate subsequently. Bacterial communities wrap themselves within the bacterial self-produced extracellular polysaccharides (EPSs), forming a highly diffusion-limiting ecosystem [4,5]. When dietary carbohydrates, such as sucrose, glucose, and fructose, are available, they are fermented by cariogenic pathogens to produce organic acids, which in turn promote the flourishing of cariogenic bacteria and ultimately create an acidic microenvironment within the biofilm (pH: 4.5–5.5) [6–8]. Consequently, the low-pH niches demineralize the structure of the tooth and lead to carious lesion formation. Thus, eliminating cariogenic bacteria and biofilms is important for preventing ECC.

The oral commensal microbiome forms a diverse, dynamic, and unique ecosystem, which is helpful for the host to defend external risks as well as prevent oral and systemic diseases [9–11]. On occasions, the imbalance of oral homeostasis could lead to dental caries, periodontitis, halitosis, and even system diseases [10,12,13]. Therefore, it is of great

significance for dentists to develop precise therapeutic methods against pathogenic biofilms without disturbing the microbiome homeostasis and surrounding mucosal tissues [14]. Recently, multiple types of pH-responsive nanoplatforms are developing [8,15–17], which could deliver drugs in the acid niches specifically. As the relatively low pH value is a distinguishing feature of cariogenic biofilms, this acid-responsive method may offer us a promising opportunity for preventing dental caries and at the same time protecting the normal oral ecosystem.

Antimicrobial photodynamic therapy (aPDT) enjoys an unflagging interest among scientists in preclinical research for oral and dental applications owing to its strong bactericidal efficiency, noninvasive nature, precise spatiotemporal control, and minimal side effects [18–21]. Current photosensitizers (PSs) used for aPDT are mainly classified into porphyrin, chlorophyll, and phthalocyanine compounds [19,22]. Among them, chlorin e6 (Ce6), an FDA-approved second-generation PS, obtained from natural chlorophyll, has demonstrated brilliant superiorities, including a high generation efficiency of reactive oxygen species (ROS), short photosensitizing period, good absorption of red light, and minimal dark toxicity [23,24]. However, despite these merits, the negative charge and poor water solubility of Ce6 greatly hamper its penetration and internalization ability in cariogenic biofilms and bacteria that possess the same charge, which are bottlenecks for its further application in the clinic [18,20,25]. In addition, microbiota-mediated biofilms possess a hyperfine structure, which provides physical and biological shelters for bacteria, protecting them against antimicrobial agents, including PSs [14,26]. Therefore, there is a tremendous need to modify PSs to enhance their penetration, retention, and internalization in highly structured cariogenic biofilms and bacteria [27].

Nanotechnology is readily expanding in the field of dentistry for infection control [28]. Among them, bioresponsive polymers have been widely used as drug carriers for combating bacteria and biofilm [8,25, 29,30]. Polyethylene glycol-*b*-poly(2-(diisopropylamino)ethyl methacrylate) (MPEG-*b*-P(DDA), MPP) is an amphiphilic and pH-responsive polymer, which could self-assemble into well-defined spherical nanostructures in neutral solution and disassemble in acidic conditions owing to the protonation of the tertiary amine [31–33]. In our previous study, MPP has been used to deliver chemotherapeutic drugs for combating cancer [32,33]. In this study, inspired by the similar acidic microenvironment of dental caries and urgency to improve the solubility and stability of Ce6, MPP loaded with Ce6 (MPP-Ce6) was constructed and used to deliver Ce6 in the cariogenic biofilm specifically. Meanwhile, the performance of MPP-Ce6-mediated aPDT for inhibiting cariogenic bacteria, biofilm, and the progression of ECC was investigated (Scheme 1).

2. Results and discussion

2.1. Rational design and characterization of MPP-Ce6

The bioresponsive release and interaction of MPP-Ce6 with cariogenic biofilm through electrostatic attraction and acidic trigger were illustrated in Fig. 1A. To develop effective strategies for eliminating cariogenic bacteria in preventing dental caries, the specific features of different cariogenic bacteria need to be investigated. In this study, the acid-producing ability and surface charges of three representative bacteria, *S. mutans*, *S. sobrinus*, and *S. sanguinis*, were explored. As shown in Fig. 1B, the pH values of different bacterial suspensions (*S. mutans*, *S. sobrinus*, *S. sanguinis*, or the mixed flora) were found to decrease continuously and ultimately reached approximately 4 in the presence of sucrose, which demonstrated the acid-producing and acid-tolerant ability of the three representative cariogenic bacteria. Cariogenic bacteria extensively aggregate in biofilms to create acidic niches [1,7,14]. Furthermore, acidic niches promote acidogenic/aciduric bacteria to thrive and prolong the period of low pH in biofilms, which leads to tooth demineralization and progression of dental caries [4,34]. In addition, the surface charges of all three cariogenic bacteria were tested to be negative, with *S. mutans* and *S. sanguinis* being approximately −30 mV and *S. sobrinus* being approximately −5 mV (Fig. 1C), indicating that
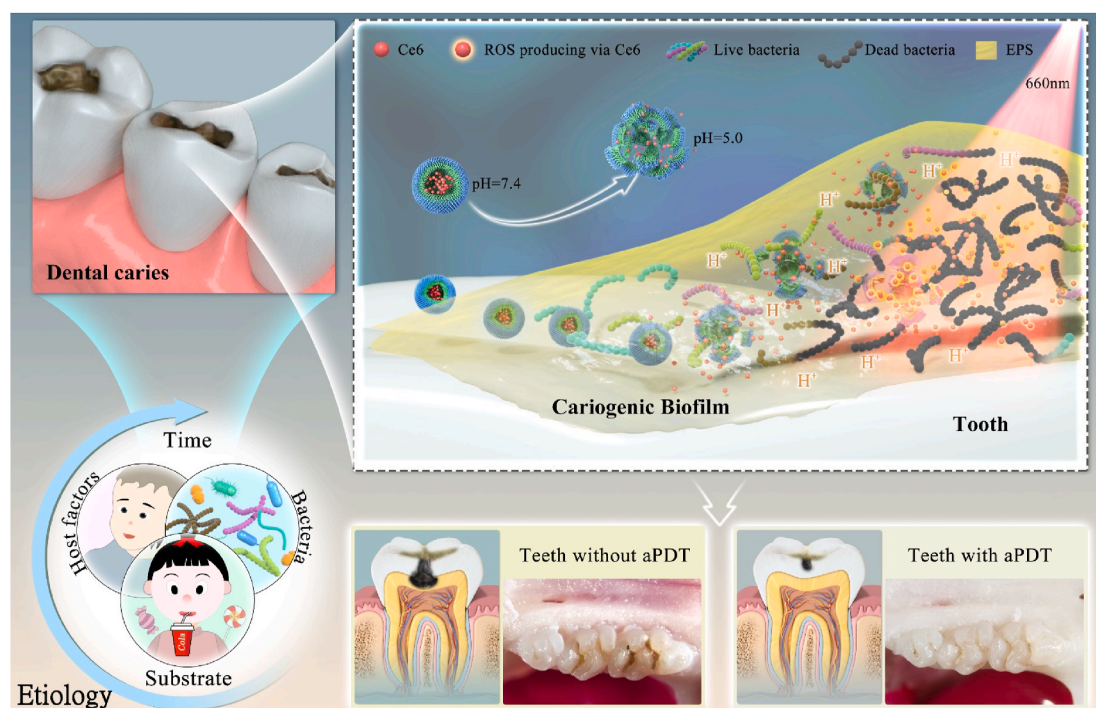
Scheme 1. Illustration of the bioresponsive polymeric nanoparticles loaded with Ce6 (MPP-Ce6) in mediating aPDT for preventing dental caries. Dental caries has multifactorial etiologies, including host factors, bacteria, substrate, and time. Cariogenic microbiota-mediated biofilms, the main factor of dental caries, create an acidic microenvironment and lead to the demineralization of teeth. The bioresponsive nanosized MPP-Ce6 could specifically release Ce6 in the microenvironment of acidic biofilms. After irradiation with a 660-nm laser, multispecies cariogenic bacteria were significantly killed, resulting in the excellent prevention efficiency of dental caries.
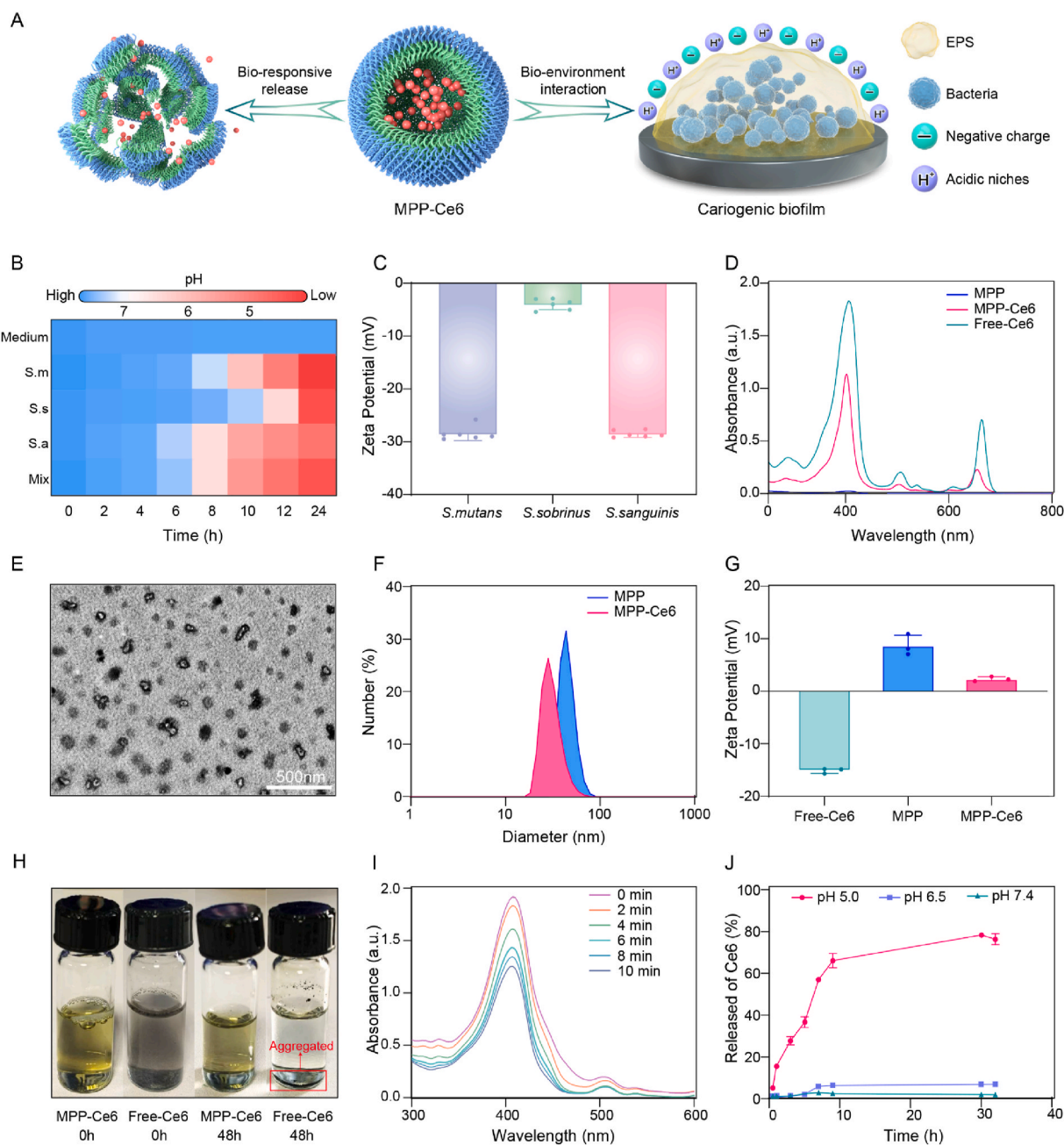
Fig. 1. Characterization of multispecies cariogenic bacteria and MPP-Ce6. A) Illustration of bioresponsive release and interaction of MPP-Ce6 with cariogenic biofilm (electrostatic attraction and acidic trigger). B) pH changes of three representative cariogenic bacteria as a function of time (Medium, brain heart infusion broth; S.m, *S. mutans*; S.s, *S. sobrinus*; S.a, *S. sanguinis*; Mix, the mixture of the abovementioned bacterial suspension). C) Zeta potentials of three representative cariogenic bacteria. D) UV–vis spectra of MPP, MPP-Ce6, and Free-Ce6. E) TEM image of MPP-Ce6. F) Size distributions of MPP and MPP-Ce6 as detected by DLS. G) Zeta potentials of MPP, MPP-Ce6, and Free-Ce6. H) Photographs of MPP-Ce6 and Free-Ce6 suspensions at 0 h and 48 h. I) ROS generation of MPP-Ce6 under the 660-nm laser as measured by UV absorption of DPBF. J) Release profiles of Ce6 from MPP-Ce6 at different pH values (pH 5.0, 6.5, and 7.4).

drugs with positive charges may be effective in targeting cariogenic bacteria. Most PSs are negatively charged and water insoluble, making them difficult to absorb into bacteria and exert their function [22,25]. Based on the abovementioned features of cariogenic bacteria and biofilms, in this work, bioresponsive polymeric nanoparticles loaded with Ce6 as a PS were designed to enhance the entrance of Ce6 into the hyperfine structure of biofilms and bacteria, which is essential for promoting the antibacterial and anti-caries efficiency of aPDT.

First, the synthesis of MPP was confirmed by ^{1}H nuclear magnetic resonance (^{1}H NMR; Fig. S1, Supporting Information). Ce6 was then loaded into the block copolymer *via* self-assembly. Contributing to the specific absorption peaks of Ce6 at 406, 506, and 663 nm, MPP-Ce6 was

confirmed to be synthesized successfully *via* UV–vis spectroscopy (Fig. 1D). The red shifting of absorption peaks for MPP-Ce6 might be related to the π-π interaction between Ce6 molecules after being encapsulated into MPP (Fig. S2, Supporting Information). Transmission electron microscopy (TEM) images revealed that the morphology of MPP-Ce6 was round and homogenous (Fig. 1E). The diameter was calculated to be approximately 60 nm *via* TEM, which was consistent with the z-average diameter (54 nm) measured by dynamic light scattering (DLS) (Fig. 1F; Table S1, Supporting Information). DLS results showed that the zeta potential of Free-Ce6 was negative. After being encapsulated into the MPP, the charge of the modified Ce6 was transformed to positive (Fig. 1G). Due to the negative charge of bacteria and

biofilms, the change in surface charge would promote the absorption of Ce6 into the biofilm and bacteria *via* electrostatic attraction [20]. In addition, the polydisperse index (PDI), loading efficiency (LE), and encapsulation efficiency (EE) of the particles are shown in Table S1, Supporting Information. The hydrophobicity and poor dispersity of many traditional PSs greatly hinder the development of aPDT [22,35]. As shown in Fig. 1H, compared with the rapid aggregation of Free-Ce6, the MPP-Ce6 solution exhibited good dispersibility and stability at 48 h. Moreover, the diameters, PDI, and zeta potentials hardly changed within 11 days, which confirmed the good stability of MPP-Ce6 and MPP (Fig. S3, Supporting Information). Thus, modified with polymeric nanoparticles, the dispersity of Ce6 could be improved, which could

overcome the difficulty of insufficient concentration at the site of biofilms. In this study, a 1,3-diphenylisobenzofuran (DPBF) probe was used to monitor the generation of ROS. As shown in Fig. 1I; Fig. S4, Supporting Information, MPP-Ce6 showed a great capability to produce ROS under 660-nm irradiation in a time-dependent manner, which indicated that MPP-Ce6 had antibacterial ability under the oxidative stress reaction.

2.2. pH-responsive release of nanoparticles

Targeting the acidic microenvironment of cariogenic biofilms, we used bioresponsive polymeric nanoparticles to achieve selective and
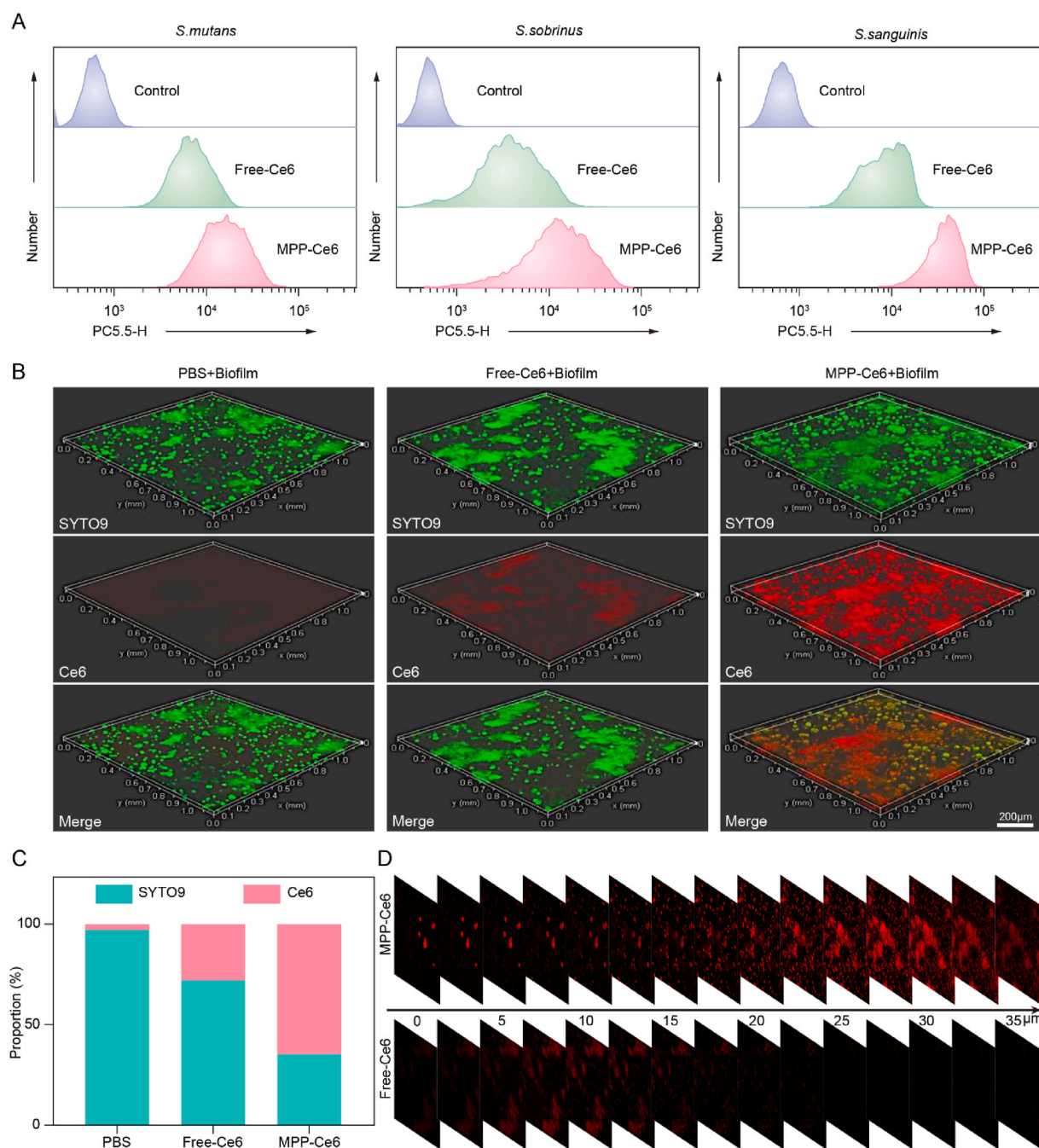

Fig. 2. Internalization and penetration of MPP-Ce6 into planktonic bacteria and biofilms. A) Uptake efficiency of MPP-Ce6 and Free-Ce6 into *S. mutans*, *S. sobrinus*, and *S. sanguinis*. B) 3D images of multispecies biofilms detected by CLSM after incubation with PBS, Free-Ce6, and MPP-Ce6 (green fluorescence, multispecies biofilm labeled by SYTO 9; red fluorescence, Ce6; scale bar, 200 μm). C) Quantification analysis to measure the proportion of fluorescence intensity of Ce6 (red) versus biofilm (green). D) The penetration depth of MPP-Ce6 and Free-Ce6 in the biofilms.

precise PSs delivery at risk sites [8,14,29]. Ideally, bioresponsive nanoparticles could bind to the pellicle and EPS surfaces but only release drugs selectively in the cariogenic biofilm triggered by its acidic pH [7,8, 14]. As shown in Fig. 1J, approximately 69% of Ce6 was burst released when the pH reached 5.0 within 9 h, 6% of Ce6 was released at pH 6.5, and almost no Ce6 was released at physiological pH (7.4). Consistent with our desire, MPP-Ce6 could release PS in a pH-dependent manner, owing to the protonation of the hydrophobic core PDA (Fig. S5, Supporting Information), which enhances the precision and specificity for drug delivery since the pH within the biofilm at active caries sites reaches 4.5–5.5 or even lower [8,36]. This "smart" release could increase the retention of PSs in situ and avoid the damage of aPDT to host oral tissues, providing new insights to improve the specific antibacterial efficiency of aPDT.

2.3. Absorption of MPP-Ce6 by planktonic bacteria and biofilms

It is essential for antimicrobial agents to penetrate biofilms deeply and be taken up by planktonic bacteria effectively to exert the antibacterial effects [37,38]. However, the hydrophobic features and poor

dispersity of Ce6 cause fluorescence quenching formation and insufficient retention in biofilms and bacteria [18,20]. Currently, polycationic polymer-modified Ce6 is highly sought to improve the retention of hydrophobic PSs in biofilm-mediated infection at at-risk sites [20,25,37]. To assess whether MPP-Ce6 could improve the absorption of Ce6 into planktonic bacteria and biofilms, flow cytometry and confocal laser scanning microscopy (CLSM) were conducted. First, the uptake efficiency of MPP-Ce6 by planktonic bacteria (*S. mutans*, *S. sobrinus*, and *S. sanguinis*) was evaluated by flow cytometry analysis. As shown in Fig. 2A, the uptake of MPP-Ce6 by the three bacteria was effectively increased compared with that of Free-Ce6. In addition, the internalization of MPP-Ce6 was upregulated in a concentration-dependent manner (Fig. S6, Supporting Information).

However, before exerting bactericidal ability, MPP-Ce6 should first penetrate deeply into the cariogenic biofilm. Thus, we further investigated the penetration depth and amount of MPP-Ce6 in the biofilm using CLSM. An *in vitro* cariogenic biofilm model was constructed and treated with Free-Ce6 or MPP-Ce6 for imaging. CLSM images and the corresponding quantitative analysis showed that the retention of MPP-Ce6 in the biofilm was approximately two times higher than that of Free-Ce6
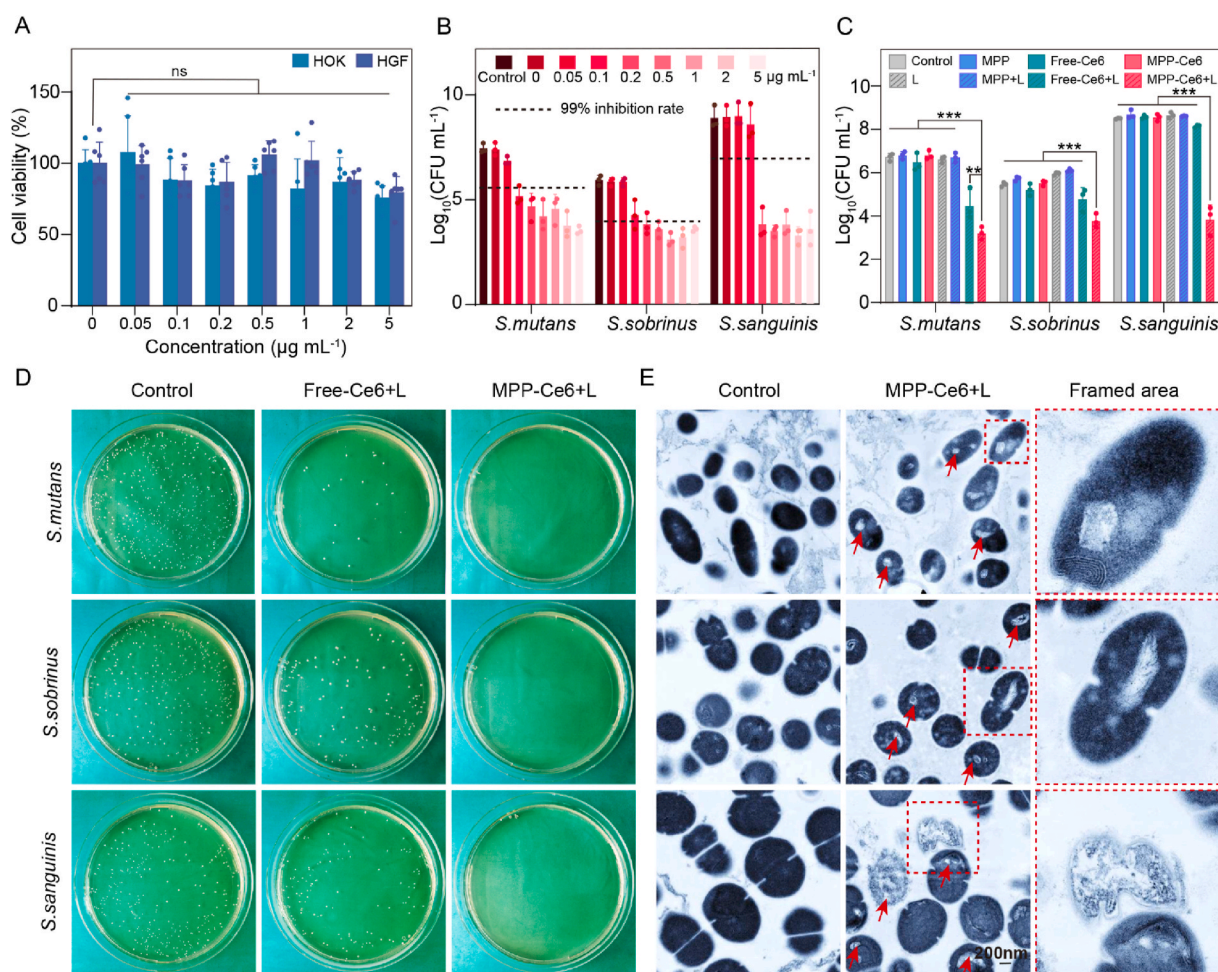

Fig. 3. Biocompatibility and antibacterial efficiency of MPP-Ce6-mediated aPDT *in vitro*. A) Cell viability of normal human oral cells (HOKs and HGFs) upon treatment with MPP-Ce6 at different concentrations (0–5 μg mL^{-1} Ce6 equivalent; ns, $p > 0.05$). B) Antibacterial efficiency of MPP-Ce6-mediated aPDT against *S. mutans*, *S. sobrinus*, and *S. sanguinis* (0–5 μg mL^{-1} Ce6 equivalent; the dotted line represents 99% inhibition rate). C) Antibacterial efficiency of different treatments against *S. mutans*, *S. sobrinus* and *S. sanguinis* (Control, treatment with BHI only; MPP, treatment with MPP only; Free-Ce6, treatment with free Ce6 only; MPP-Ce6, treatment with MPP-Ce6 only; L, treatment with laser only; MPP+L, treatment with MPP upon laser irradiation; Free-Ce6+L, treatment with free Ce6 upon laser irradiation; MPP-Ce6+L, treatment with MPP-Ce6 upon laser irradiation; concentration of MPP-Ce6 and free Ce6, 0.1 μg mL^{-1} Ce6 equivalent for *S. mutans*, 0.2 μg mL^{-1} Ce6 equivalent for *S. sobrinus* and *S. sanguinis*; **, $p < 0.01$; ***, $p < 0.001$). D) Representative images of three species of bacterial colonies in the Control, Free-Ce6+L, and MPP-Ce6+L groups (dilution factors of 1:10^4 for *S. mutans*, 1:10^3 for *S. sobrinus*, and 1:10^6 for *S. sanguinis*). E) Morphological changes in bacteria treated with or without MPP-Ce6 upon laser irradiation by TEM (red arrows indicate the destruction of the bacterial structure; framed areas are enlarged on the right; scale bar, 200 nm).

(Fig. 2B and C). The penetration depth of Free-Ce6 in the biofilm was observed to be only 20 μm. Of note, MPP-Ce6 could increase the penetration depth by more than 75% (>35 μm), which provides a prerequisite for killing bacteria at deep biofilm depths (Fig. 2D).

2.4. Antibacterial efficiency of MPP-Ce6-mediated aPDT

The biocompatibility of MPP-Ce6 was first confirmed by the cell counting kit-8 (CCK-8) test. As shown in Fig. 3A, after incubation with different concentrations of MPP-Ce6 for 24 h in the dark, more than 75% of normal cells (human oral keratinocytes, HOKs; human gingival fibroblasts, HGFs) still survived. Based on the excellent ROS generation efficiency, largely enhanced biofilm penetration, and increased bacterial internalization capability, the bactericidal activities of MPP-Ce6-mediated aPDT against the three representative cariogenic bacteria (*S. mutans*, *S. sobrinus,* and *S. sanguinis*) were then investigated. As depicted in Fig. 3B, the three cariogenic bacteria were effectively killed by MPP-Ce6-mediated aPDT in a dose-dependent manner, with a more than 99% inhibition rate at a relatively low concentration (loaded with 0.1 or 0.2 μg mL^{-1} Ce6). Afterwards, experiments were conducted to compare the bactericidal activity of MPP-Ce6-mediated aPDT with other groups (Fig. 3C and D; Fig. S7, Supporting Information), where the corresponding concentrations of Ce6 that induced a 99% bacterial inhibition rate were selected for analysis (0.1 μg mL^{-1} for *S. mutans*; 0.2 μg mL^{-1} for *S. sobrinus* and *S. sanguinis*). The results showed that, compared with other groups, MPP-Ce6 with light illumination exhibited a much better antibacterial ability.

To further explore the bactericidal mechanism of MPP-Ce6-mediated aPDT, the structural and morphological changes of cariogenic bacteria were observed by TEM. As shown in the left panel of Fig. 3E, all three species of bacteria in the control group were spherical-shaped with a distinguishable and intact structure. However, after being treated with MPP-Ce6-mediated aPDT, the integrality of the bacterial structure was destroyed, and the cell walls tended to be irregular and wrinkled. Moreover, many holes were observed in all three species of bacteria, which might have resulted from the leakage of intracellular contents [39]. Consistent with other studies, aPDT could destroy the proteins, membrane lipids, and cell walls of bacteria [40]. Therefore, MPP-Ce6-mediated aPDT might successively induce the destruction of bacterial structures, leakage of intracellular contents, and ultimately cause bacterial death.

2.5. Anti-biofilm efficiency of MPP-Ce6-mediated aPDT

In the clinic, cariogenic biofilms hinder the entrance of antimicrobial agents into their deep structure and eventually result in treatment failure [14]. To investigate the antibiofilm efficiency of MPP-Ce6-mediated aPDT, *S. mutans*, *S. sobrinus*, and *S. sanguinis* were selected to successfully construct multispecies biofilms, which were verified *via* fluorescent in situ hybridization (FISH) analysis (Fig. 4A). *S. sanguinis* could act as a "pioneer" to colonize the salivary pellicle-coated tooth at an early stage and communicate with other cariogenic bacteria through specific receptors on its surface, which is essential for biofilm formation [4,41]. As shown in the biofilm model (Fig. 4A), the population of *S. sanguinis* (red) was predominant in the whole three-dimensional (3D) structure of the biofilm. Additionally, *S. mutans* (green) and *S. sobrinus* (blue), as the main acid and EPS producers, were dispersedly embedded into the "scaffold" formed by *S. sanguinis* (Fig. 4A). Moreover, *S. mutans* colocalized with *S. sobrinus* in the biofilm (Fig. 4A), which indicated that the two species might have a symbiotic relationship and accelerate the progression of caries when combined [42,43].

After multispecies biofilms were successively constructed, biofilm eradication and biofilm inhibition efficiency of MPP-Ce6 mediated aPDT were further evaluated (Fig. 4B). First, to explore the therapeutic ability of MPP-Ce6-mediated aPDT against multispecies biofilms, a 12-h-old biofilm was prepared and then treated with MPP-Ce6 plus 660-nm

light illumination. Live/dead bacterial staining was then performed, and the results showed that bacteria in the multispecies biofilm were effectively killed by MPP-Ce6-mediated aPDT in a dose-dependent manner (Fig. 4C). To determine whether the preformed biofilm would also be eliminated by MPP-Ce6-mediated aPDT, crystal violet staining was performed to quantify the biofilm biomass after different treatments (Fig. S8, Supporting Information). The results showed that aPDT had no effect on eliminating the preformed biofilm, which is attributed to the complex structure of the biofilm constituted with microbes and EPS [14]. Although the pre-formed biofilm was hardly disrupted after MPP-Ce6-mediated aPDT, the cariogenic bacteria, which produce the acid and virulence factors, had been blocked, preventing further tooth damage. Second, to investigate the ability of MPP-Ce6-mediated aPDT to inhibit the formation of cariogenic biofilms, treatments were conducted throughout the biofilm progression (every 24 h, three times), which is consistent with daily oral hygiene activities. For field–emission scanning electron microscopy (FE-SEM) analysis, a cariogenic biofilm was constructed on saliva-coated hydroxyapatite (sHA) to mimic the true oral environment.

As shown in the control group of Fig. 4D, the cariogenic biofilm without any treatments had a complex porous 3D microstructure, where microbial communities possessing a beaded structure were embedded into the EPS scaffold. However, in the MPP-Ce6+Laser groups, the biofilms were sharply reduced, and the number of bacteria was significantly decreased in a concentration-dependent manner (Fig. 4D). Consistently, crystal violet staining results confirmed the downregulation of biofilm biomass (Fig. 4E and F). In addition, the level of water-insoluble polysaccharide, which reflects the number of EPS in biofilms, was measured *via* anthrone assay. The results showed that water-insoluble glucan was also reduced after MPP-Ce6-mediated aPDT (Fig. 4G). These results suggest that MPP-Ce6-mediated aPDT not only kills the bacteria in preformed biofilms but also inhibits biofilm formation by repressing bacterial progression and EPS production. In addition, the three concentrations of MPP-Ce6 were chosen in this part *via* gradient concentration tests previously performed (Fig. S9, Supporting Information).

2.6. MPP-Ce6-mediated aPDT for dental caries in vivo

To further verify the effectiveness of MPP-Ce6-mediated aPDT *in vivo*, 15-day-old rats were used to establish a rodent caries model to mimic ECC [8,16]. From day 21, MPP-Ce6-mediated aPDT and other treatments were performed for three consecutive days and then applied every two days. During the process of caries model establishment and aPDT treatments, oral sampling and colony-forming unit (CFU) counting were conducted regularly to monitor the population of cariogenic microbes (Fig. S10, Supporting Information). After rats were sacrificed, carious lesions were assessed *via* Keyes' scoring and micro-CT analysis (Fig. 5A). As shown in the upper panel of Fig. 5B, no bacterial colonies on selective media were found in the first sampling at day 17, indicating that the indigenous oral microorganisms were effectively inhibited after antibiotic treatments. After inoculation of cariogenic bacteria for three consecutive days, the colonization of *Streptococcus spp.* reached approximately 1×10^5 CFU mL^{-1} at day 20, suggesting that bacterial infection was well established (Fig. 5B and C). Subsequently, during the treatments of MPP-Ce6-mediated aPDT, more than 90% of the cariogenic organisms were inhibited (reduced by 1 log unit, Fig. 5B,D; Fig. S11, Supporting Information), whereas the bacterial number of the Free-Ce6+Laser group decreased slightly, which indicated the superb antibacterial effects of MPP-Ce6-mediated aPDT *in vivo*. The specific sampling results of every rat and the statistical significance of antibacterial efficiency are also presented (Fig. 5D). Based on the outstanding antibacterial efficiency of MPP-Ce6+Laser treatment *in vivo*, we speculated that MPP-Ce6-mediated aPDT might also inhibit the progression of dental caries. The morphology and color of the teeth collected at day 47 indicated that most of the lesions on the teeth were pit-and-fissure caries
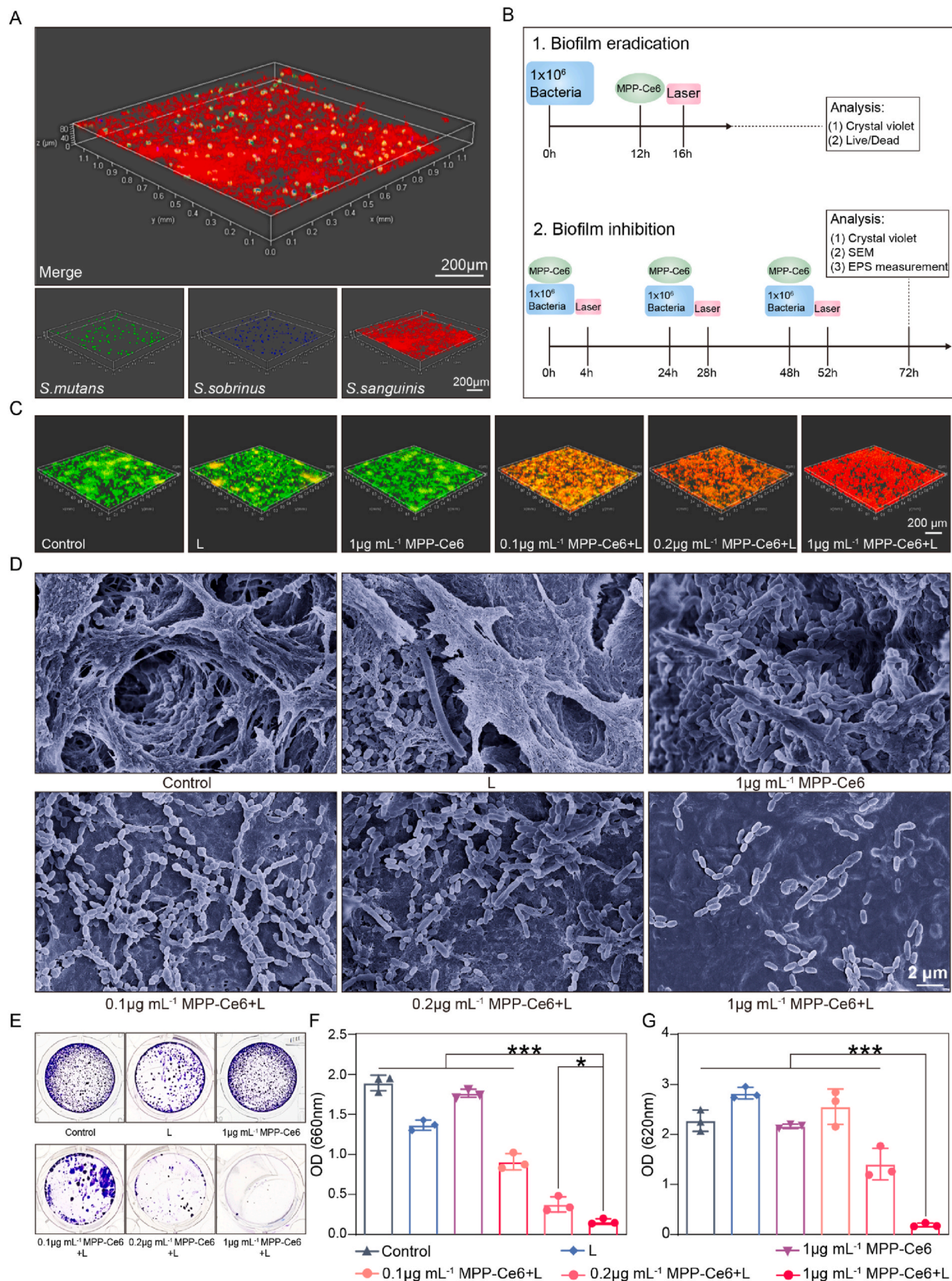
Fig. 4. Antibiofilm efficiency of MPP-Ce6-mediated aPDT *in vitro*. A) Construction of multispecies biofilms detected by FISH analysis (scale bar, 200 μm; green, *S. mutans*; blue, *S. sobrinus*; red, *S. sanguinis*). B) Scheme of dual-mode antibiofilm efficiency (biofilm eradication test and biofilm inhibition test). C) Live/dead bacterial staining of multispecies biofilms after different treatments for the biofilm eradication test (scale bar, 200 μm; green, live bacteria; red, dead bacteria; Control, treatment with BHI only; L, treatment with laser only; MPP-Ce6, treatment with MPP-Ce6 only; MPP-Ce6+L, treatment with MPP-Ce6 upon laser irradiation). D) FE-SEM images, E) crystal violet staining, F) crystal violet staining's quantification results, and G) water-insoluble polysaccharide measurements of multispecies biofilms after different treatments for the biofilm inhibition test (scale bar, 2 μm; *, $p < 0.05$; ***, $p < 0.001$).
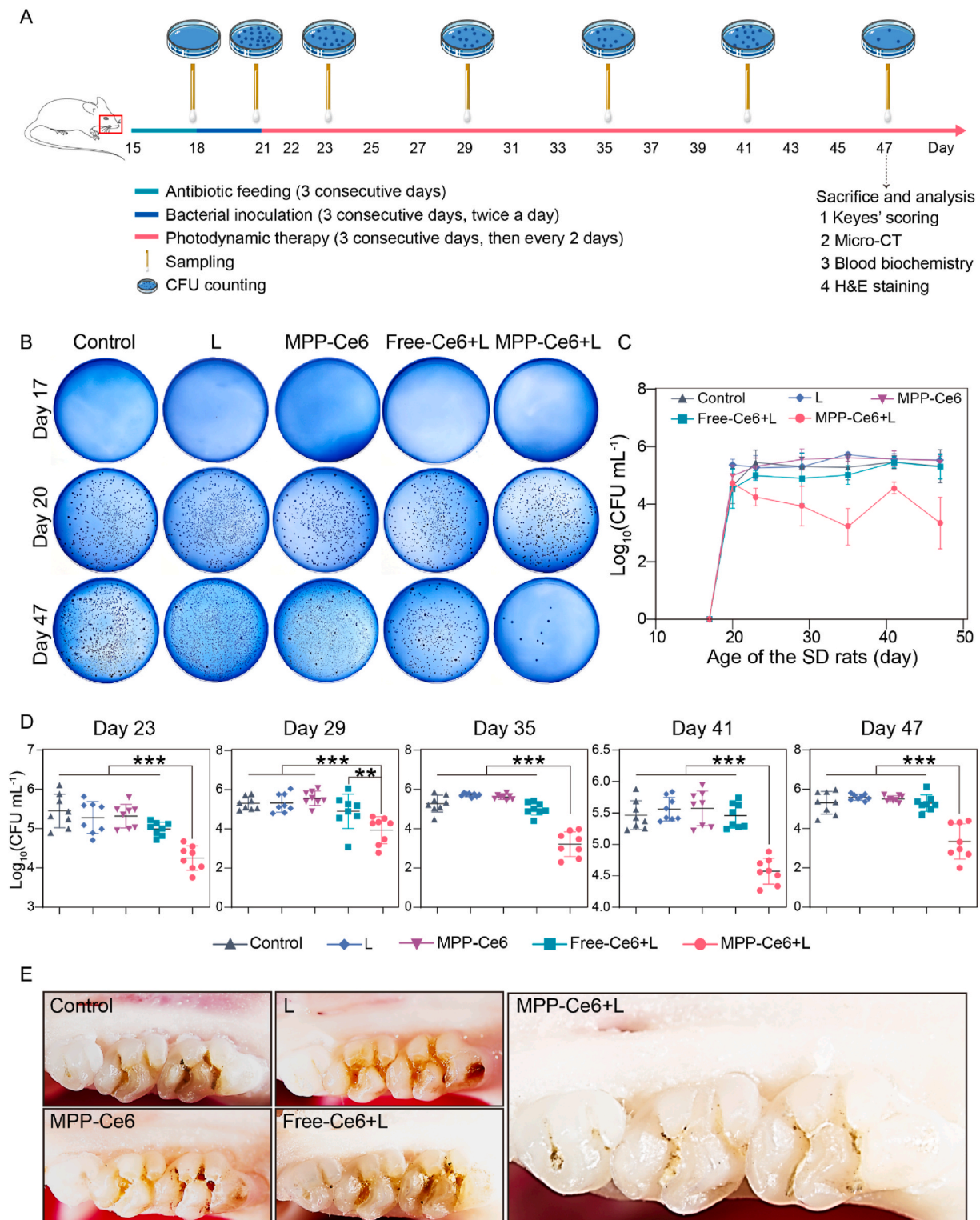
Fig. 5. *In vivo* assessment of MPP-Ce6-mediated aPDT for dental caries. A) Schedule of rodent caries model construction, therapeutic approaches with different treatments, and assessments of antibacterial/anti-caries efficacy. B) Representative images of surviving bacterial colonies on MSB agar plates for different treatment groups at 17, 20, and 47 days (Control, treatment with BHI only; L, treatment with laser only; MPP-Ce6, treatment with MPP-Ce6 only; Free-Ce6+L, treatment with free Ce6 upon laser irradiation; MPP-Ce6+L, treatment with MPP-Ce6 upon laser irradiation). C) CFU counting for surviving bacterial colonies at 17, 20, 23, 29, 35, 41, and 47 days. D) Statistical analysis of surviving bacterial colonies after MPP-Ce6-mediated aPDT (**, $p < 0.01$; ***, $p < 0.001$). E) Representative photographs upon stereoscopic microscopy of the occlusal surface of rodent teeth treated as noted at day 47.

(Fig. 5E), which was similar to dental caries that happens in humans. Moreover, compared with other groups, carious lesions in the MPP-Ce6+Laser group were smaller, and the enamel surfaces were more integrated (Fig. 5E).

To further quantify the specific caries-preventing effects of MPP-Ce6-mediated aPDT, Keyes' scoring and micro-CT analysis were conducted to evaluate the depth and degree of carious lesions in different groups [8,16,44]. As shown in Fig. 6A, murexide staining (red) was used to label the area and depth of carious lesions according to Keyes' scoring, which were divided into the following four levels: enamel only (E), slightly

dentinal (Ds, <1/4 of the dentin region), moderate dentinal (Dm, 1/4–3/4 of the dentin region), and extensive dentinal (Dx, >3/4 of the dentin region) [45,46]. Importantly, the staining results showed that the severity of carious lesions was sharply decreased in the MPP-Ce6+Laser group (Fig. 6A). Quantification results showed that the scoring of E on the smooth surface was significantly decreased in the MPP-Ce6+Laser group (Fig. 6B). Moreover, the severity of carious lesions on the sulcal surface was quantified based on four levels, including total lesions (E+Ds+Dm+Dx), initial lesions (Ds+Dm+Dx), moderate lesions (Dm+Dx), and extensive lesions (Dx) (Fig. 6C), where total lesions
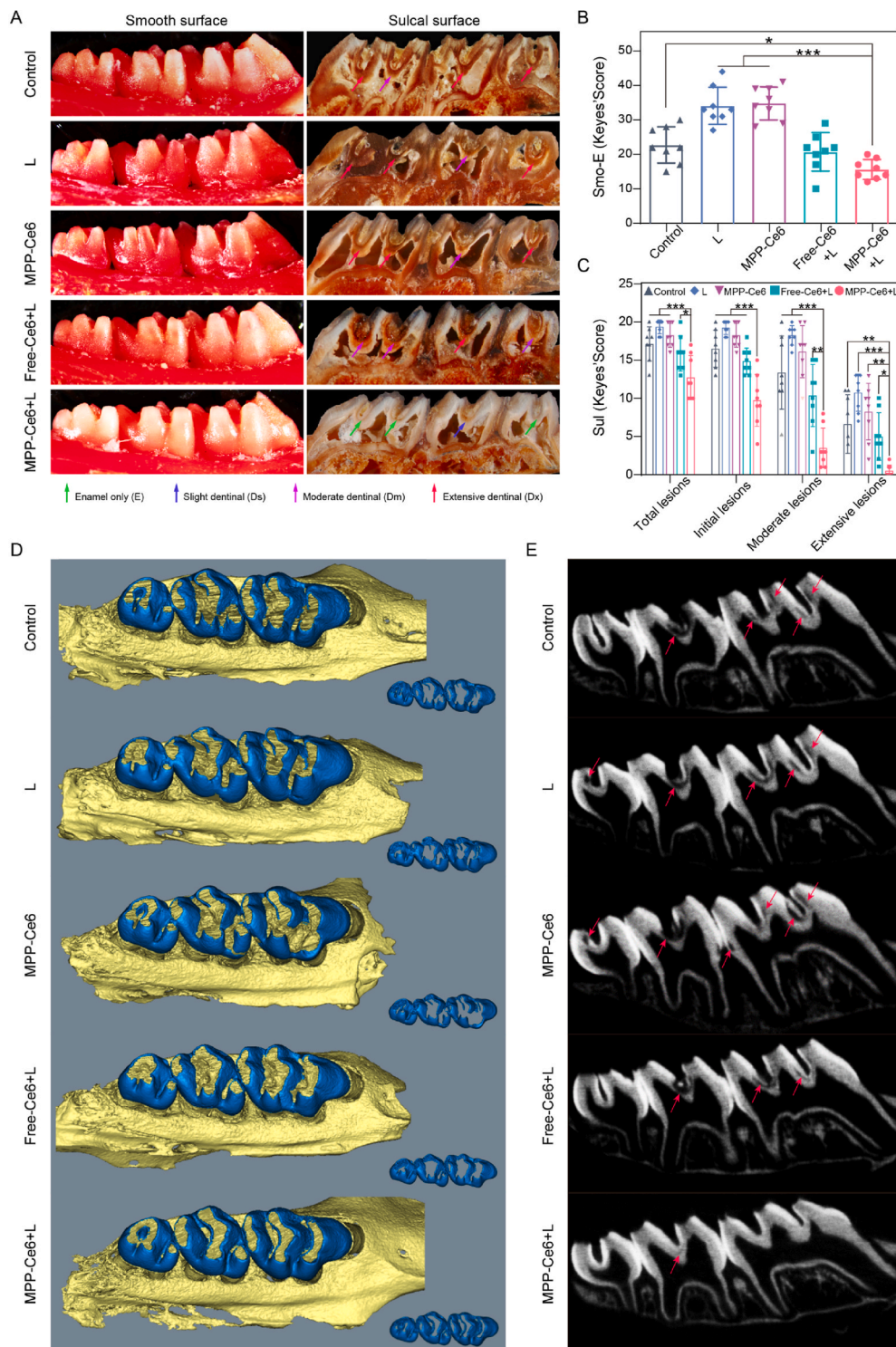

Fig. 6. Anti-caries efficacy after different treatments as evaluated by Keyes' scoring and micro-CT analysis. A) Representative images of carious lesions stained by murexide (60 mg mL^{-1}) on the smooth surface and sulcal surface with teeth of different severities (green arrows, affected enamel only, E; blue arrows, affected slight dentinal, within 1/4 of the dentin, Ds; purple arrows, affected moderate dentinal, 1/4–3/4 of the dentin, Dm; red arrows, affected extensive dentinal, beyond 3/4 of the dentin, Dx; Control, treatment with BHI only; L, treatment with laser only; MPP-Ce6, treatment with MPP-Ce6 only; Free-Ce6+L, treatment with free Ce6 upon laser irradiation; MPP-Ce6+L, treatment with MPP-Ce6 upon laser irradiation). B) and C) Statistical analysis of Keyes' scoring on the smooth surface and sulcal surface based on the depth and extent of carious lesions (total lesions, E+Ds+Dm+Dx; initial lesions, Ds+Dm+Dx; moderate lesions, Dm+Dx; extensive lesions, Dx; *, $p < 0.05$; **, $p < 0.01$; ***, $p < 0.001$). D) 3D reconstruction of micro-CT images of maxillary molars in different groups, separated enamel (blue) by setting the density threshold above 11000 Hounsfield units. E) 2D scale sagittal images of the maxillary molars analyzed by micro-CT (red arrows, caries lesion sites).

represent the incidence of caries and others indicate the severity of caries. Remarkably, the incidence and severity of caries were significantly reduced in the MPP-Ce6+Laser group (Fig. 6C).

Acid-producing bacteria-induced demineralization of the tooth is one of the most important features of dental caries, and can be visualized by micro-CT as a supplemental method to analyze carious lesions [44, 47]. As presented in Fig. 6D, the teeth in the MPP-Ce6+Laser group had more intact enamel (blue), which was stripped and reconstructed from the maxillary molars. Moreover, the enamel in the MPP-Ce6+Laser group had fewer demineralization sites (shadows marked by red arrows) according to the corresponding sagittal slice images (Fig. 6E). However, for the other groups, the number and area of demineralization sites in the pit and fissure were more extensive and even reached the pulp cavity, indicating the serious destruction of dental tissue in these groups. The above results demonstrated that MPP-Ce6-mediated aPDT was efficient at killing multispecies cariogenic bacteria and preventing the progression of dental caries.

The biocompatibility of MPP-Ce6-mediated aPDT *in vivo* was assessed *via* histological analysis of the oral mucosa and main organs, body weight monitoring, and blood biochemistry detection. First, to prove the safety of treatments on the tissue near the irradiation site, tongue and palate mucosa were collected for hematoxylin and eosin (H&E) staining (Fig. 7A), where no oral mucosa diseases, such as hyperemia, erosion, ulcer, inflammation, hydrops, and necrosis, were observed after different treatments. During the treatment period, the body weights of the rats continuously grew and no difference was observed among the five groups (Fig. 7B). In addition, blood biochemistry analyses were conducted to assess renal and liver function. Alanine aminotransferase (ALT), aspartate aminotransferase (AST), and alkaline phosphatase (ALP) in serum were measured to assess liver function, and no significant difference was observed for the MPP-Ce6+Laser group compared with the other groups (Fig. 7C–E). Additionally, no significance was detected among the different groups concerning renal function, which was indicated by the levels of blood urea nitrogen (BUN) and serum creatinine (CREA) (Fig. 7F and G). Furthermore, the histopathological structures of the major organs (heart, liver, spleen, lung, and kidney) remained unchanged in all groups (Fig. S12, Supporting Information). These results demonstrated that MPP-Ce6-mediated aPDT is a biocompatible way to inhibit dental caries progression.

3. Conclusion

In this work, a simple but efficient method was developed to combat cariogenic bacteria for preventing dental caries. In particular, a conventional PS, Ce6, was encapsulated into a bioresponsive nanoparticle, triggering the release of Ce6 in the acidic microenvironment within the cariogenic biofilm. Owing to the excellent dispersity and stability, small size, and negative to positive charge conversion of MPP-Ce6, the uptake
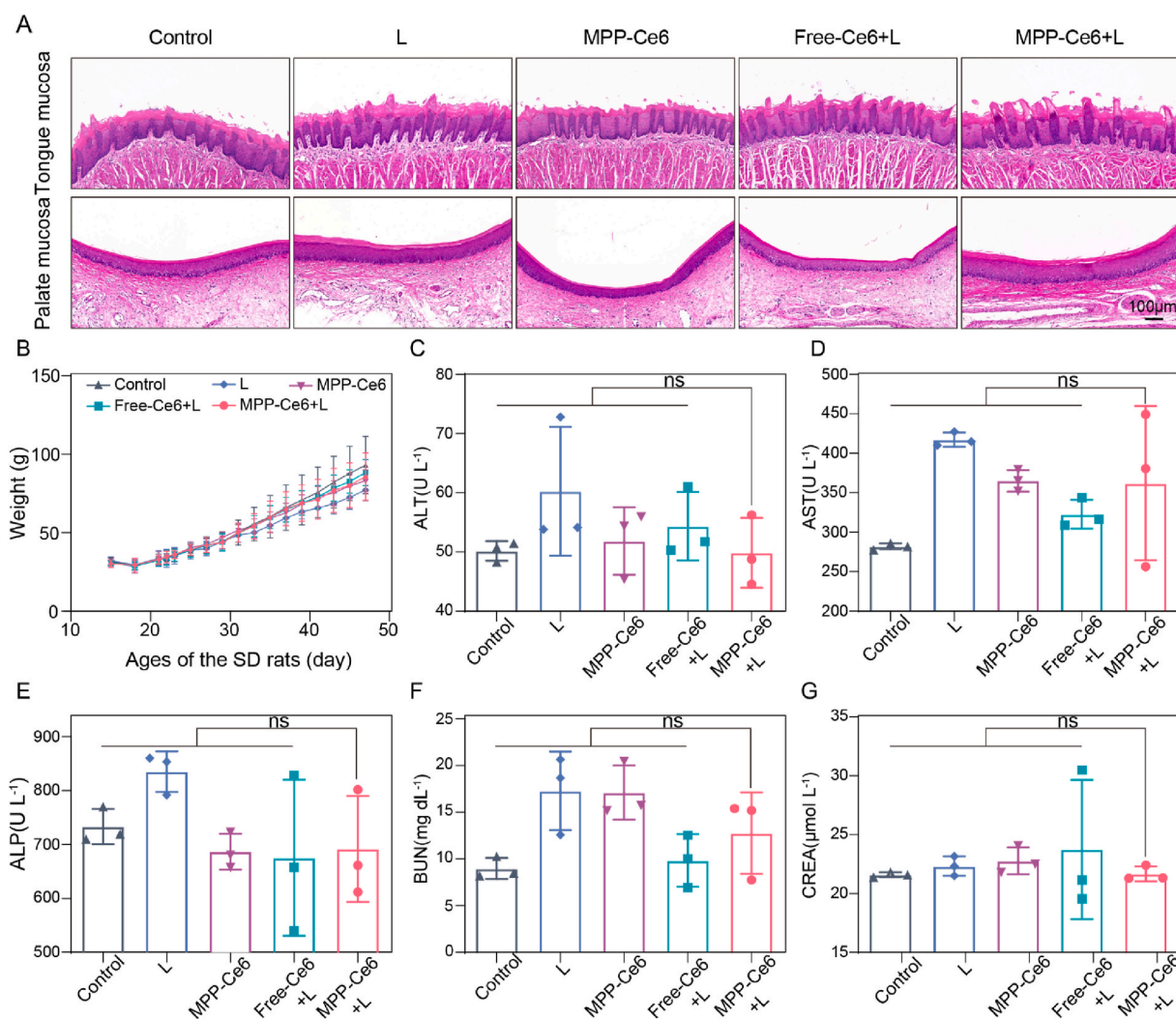

Fig. 7. Biocompatibility of MPP-Ce6-mediated aPDT *in vivo*. A) H&E staining of the oral mucosa from different groups (scale bar, 100 μm). B) Body weight changes of rats with different treatments. C-G) Blood biochemistry analysis of liver function (ALT, AST, and ALP) and kidney function (BUN and CRET) (ns, $p > 0.05$).

efficiency of MPP-Ce6 in cariogenic bacteria as well as the penetration of MPP-Ce6 in the cariogenic biofilm were drastically enhanced. Importantly, MPP-Ce6-mediated aPDT exhibited a strong antibacterial efficiency against *S. mutans*, *S. sobrinus*, and *S. sanguinis in vitro*. Moreover, MPP-Ce6-mediated aPDT exhibited outstanding antibiofilm efficiency, which not only killed the bacteria in mature biofilms but also inhibited multispecies biofilm formation *in vitro*. Furthermore, in an ECC rodent model, MPP-Ce6-mediated aPDT remarkably inhibited the growth of cariogenic bacteria and significantly reduced the number and severity of carious lesions, indicating that multispecies bacteria-induced ECC could be controlled and prevented effectively. In addition, MPP-Ce6-mediated aPDT resulted in no signs of adverse effects on host tissues *in vivo*. For clinical translation, we speculate that this promising therapeutic approach would be useful in the management of ECC. MPP-Ce6 could be added into toothpaste or mouthwash, which can be combined with a laser attached to an electric toothbrush or water flosser. This is quite promising to promote the cleaning efficiency of traditional oral hygiene in the control and prevention of biofilm-associated dental caries.

4. Experimental section

Materials: Ce6 was obtained from J&K Scientific Ltd. Poly (ethylene glycol) methyl ether (MPEG, $M_n = 2000$), PDA, dimethyl sulfoxide (DMSO), N, N-dimethylformamide (DMF), DPBF, and aluminum oxide (Al_2O_3) were purchased from Sigma-Aldrich Chemical Co., Llc. Triethylamine (TEA, 99%), 2-bromoisobutyryl bromide (BIBB, 98%), copper (I) bromide (CuBr, 99%), and bacitracin were obtained from Shanghai Aladdin Bio-chem Technology Co., Ltd. Brain heart infusion (BHI) broth was obtained from Beijing Land Bridge Technology Co., Ltd. Mitis salivarius agar and potassium tellurite were purchased from Shandong Tuopu Biol-Engineering Co., Ltd. CCK-8 was obtained from Dojindo Laboratories. Sucrose, crystal violet, and anthrone were purchased from Sinopharm Chemical Reagent Co., Ltd.

Bacterial strains: Three standard bacterial strains were used in the antibacterial experiments. *S. mutans* (UA159 & ATCC 700610), *S. sobrinus* (ATCC 27352), and *S. sanguinis* (SK36 & ATCC BAA-1455D-5) were resuscitated in BHI broth and cultured overnight under microaerobic conditions with 5% CO_2 at 37 °C. The optical density (OD) value of the bacterial suspension at 600 nm was adjusted to 0.8 (1×10^9 CFU mL^{-1}). BHI agar as a solid medium was used for the growth of monoclonal bacterial colonies. For the cariogenic animal experiment, dental plaques were acquired using oral swabs and then dispersed in phosphate-buffered saline (PBS; HyClone) *via* sonication. As a selective medium, mitis salivarius agar with bacitracin (0.2 units mL^{-1}) and potassium tellurite (0.01 mg mL^{-1}; MSB agar) was used for isolation of *Streptococcus spp*.

Cell lines: HGFs (ATCC) and HOKs (ATCC) were used as normal cells in the cytotoxicity assay. HGFs were cultured in α-Minimum Eagle Medium (α-MEM; HyClone). HOKs were cultured in Dulbecco's Modified Eagle Medium (DMEM) containing high glucose (HyClone). The abovementioned cell culture media was supplemented with 10% fetal bovine serum (FBS; Gibco) and 1% penicillin/streptomycin (P/S; Gibco). Cells were cultured at 37 °C with 5% CO_2.

pH changes in the bacterial suspension: Two milliliters (1×10^7 CFU mL^{-1}; n = 3) of the bacterial suspension (*S. mutans*, *S. sobrinus*, *S. sanguinis*, or mixture of the abovementioned) was added to BHI broth (20 mL) with 1% sucrose. At 2 h, 4 h, 6 h, 8 h, 10 h, 12 h, and 24 h, bacterial suspension (2 mL) was removed for pH measurement.

Zeta potentials of bacteria: The bacterial suspension (1×10^9 CFU mL^{-1}; n = 6) was diluted 100-fold with double-distilled water (ddH₂O). Then, the zeta potentials of bacteria were assessed using DLS (Nano ZS90 Malvern).

Preparation of nanoparticles: MPP was synthesized according to our previous report [33]. To prepare MPP-Ce6, first, MPP (10 mg) and Ce6 (1 mg) were dissolved in DMSO (1 mL). Afterwards, DMSO was dropped into the reaction flask containing 2 mL of water along with ultrasonic

vibration and stirred for 30 min. Finally, the mixture was transferred to a dialysis bag (MW = 3500) and dialyzed for 48 h.

Characterization of nanoparticles: The hydrodynamic diameters and zeta potentials of MPP and MPP-Ce6 were measured by DLS at 25 °C. TEM (JEM-2100) was used to observe the structure of MPP-Ce6 diluted on the copper grid. Then, one hundred particles were randomly selected to calculate the diameter of MPP-Ce6 in TEM. MPP-Ce6 and Free-Ce6 was dispersed in ddH₂O at RT, respectively. Subsequently, photographs were recorded at 0 h and 48 h to determine the dispersity of the nanoparticles. In addition, the hydrodynamic diameters and zeta potentials of the nanoparticles at 1, 3, 5, 7, 9, and 11 days were measured to evaluate the stability of MPP-Ce6.

Drug loading: The amount of Ce6 loaded in MPP-Ce6 was measured using a microplate reader (Tecan SPARK-10 M; excitation/emission wavelength, Ex/Em, 405/600 nm). First, the prepared nanoparticles (50 μL) were redistributed into water (2.95 mL; HCl concentration, 0.1 mol L^{-1}) and stirred for 48 h in the dark. Afterwards, the concentration of Ce6 was read by a microplate reader. In addition, the LE% and EE% were calculated according to the following formulas:

LE (%) = weight of Ce6 encapsulated in MPP-Ce6/weight of MPP-Ce6 × 100%

EE (%) = weight of Ce6 encapsulated in MPP-Ce6/weight of Ce6 in feed × 100%

pH-responsive release: The drug release behavior of MPP-Ce6 was investigated in different PBS buffers (pH = 7.4, 6.5, or 5.0) at 37 °C. Briefly, MPP-Ce6 (1 mL; loaded with 100 μg mL^{-1} Ce6) was added into a dialysis bag and then placed in different PBS buffers (30 mL). At selected time points, suspension (1 mL) was removed from the PBS buffer, and fresh medium (1 mL) was added to the solution outside of the dialysis bag. Finally, the concentration of Ce6 was measured using a microplate reader.

ROS generation in vitro: DPBF reagent was used to explore the ROS generation efficiency of MPP-Ce6 *in vitro*. MPP-Ce6 (loaded with 5 μg mL^{-1} Ce6) or PBS (pH 7.4) was first mixed with DPBF solution (1 mg mL^{-1} in DMF). Then, the liquid was irradiated with a 660-nm laser (LWRPD-1.5F, Laserwave Co., Ltd; 0.5 W cm^{-2}), and the fluorescence signal at 410 nm was recorded at specific time points (0, 2, 4, 6, 8, and 10 min) [48]. Additionally, the absorbance of the fluorescence signal without laser irradiation was set as F_0.

Uptake efficiency of MPP-Ce6 into planktonic bacteria: To investigate the uptake efficiency of MPP-Ce6 and Free-Ce6 into the planktonic bacteria, different species of bacterial suspension (1×10^8 CFU mL^{-1}) were cultured with MPP-Ce6 (loaded with 10, 2, or 0.2 μg mL^{-1} Ce6) or Free-Ce6 (10, 2, or 0.2 μg mL^{-1} Ce6) for 5 h. The bacterial suspension with PBS treatment served as a negative control. Then, the liquid was transferred into a centrifuge tube. Furthermore, bacteria were recovered by centrifugation at 15,000 rpm for 15 min. After washing three times, bacteria were resuspended and evaluated by flow cytometry (Beckman Coulter, USA).

Penetration of MPP-Ce6 into the biofilm: First, a multispecies cariogenic biofilm was constructed by coculturing *S. mutans, S. sobrinus,* and *S. sanguinis* on a cover glass for 12 h. Then, the biofilm was cultured with fresh BHI broth (1% sucrose) containing MPP-Ce6 (loaded with 10 μg mL^{-1} Ce6) or Free-Ce6 (10 μg mL^{-1} Ce6) for 4 h. After it was washed three times with saline, SYTO 9 was used to label bacteria in the biofilm. The penetration of MPP-Ce6 or Free-Ce6 in the biofilm was evaluated by detecting Ce6 and SYTO 9 (Ex/Em: 485/498 nm) using CLSM (Leica sp8, Germany) with a distance of 0.5 μm between each image. The fluorescence intensities of SYTO 9 and Ce6 were quantified, and the ratio was calculated using ImageJ software (n = 10).

Cytotoxicity of MPP-Ce6: The CCK-8 test was used to measure the cytotoxicity of MPP-Ce6 on human normal oral cells (HGFs and HOKs). Cells were seeded into a 96-well plate (5×10^4 cells $well^{-1}$) and cultured for 24 h. The suspension was replaced by fresh media containing

different concentrations of MPP-Ce6 (loaded with 0, 0.05, 0.1, 0.2, 0.5, 1, 2, and 5 μg mL^{-1} Ce6; n = 6) and cultured for 24 h in the dark. Then, the cells were incubated with 10% CCK-8 reagent for 40 min in the dark. The OD values at 450 nm were evaluated using a microplate reader (Power Wave XS2, BioTek Instruments).

aPDT of MPP-Ce6 against planktonic bacteria: The bacterial suspension (1 × 10^7 CFU mL^{-1}) was incubated with MPP-Ce6 at the concentrations described in the "Cytotoxicity of MPP-Ce6". After incubation for 4 h, the bacterial suspension was irradiated with a 660-nm laser (0.5 W cm^{-2}) for 5 min. Then, the bacterial suspension was inoculated on BHI agar after dilution. Forty-eight hours later, CFU counting was calculated based on the dilution factors and the number of monoclonal bacterial colonies. The corresponding concentrations of MPP-Ce6, which have a 99% bactericidal rate, were used to further evaluate the antibacterial efficiency of different treatments.

The antibacterial efficiencies of MPP-Ce6, Free-Ce6, MPP, and BHI with or without laser were determined according to the aforementioned method. MPP-Ce6 loaded with 0.1 μg mL^{-1} Ce6 was used for the planktonic *S. mutans* test and loaded with 0.2 μg mL^{-1} Ce6 for the *S. sobrinus* and *S. sanguinis* tests. The concentrations of Free-Ce6 were consistent with the MPP-Ce6 loaded (n = 3).

Morphological changes of the bacteria after aPDT: To explore the antibacterial mechanism of MPP-Ce6 after aPDT, the morphology and structure of the planktonic bacteria were observed. Briefly, after the aPDT treatment mentioned above, bacteria were collected and fixed overnight with 2.5% glutaraldehyde at 4 °C. Finally, samples were observed by TEM. Bacteria without any treatment were used as a control group.

Construction of multispecies biofilm: Two types of biofilm models were constructed to confirm the effects of biofilm eradication and biofilm inhibition after MPP-Ce6-mediated aPDT. First, *S. mutans*, *S. sobrinus*, and *S. sanguinis* at the same concentration (1 × 10^6 CFU mL^{-1}) and volume (200 μL) were mixed in BHI broth supplemented with 1% sucrose. To establish a model of biofilm eradication, bacterial compound (300 μL) was inoculated into a well for a period of time. After removal of the medium, MPP-Ce6 at different concentrations was added to the wells (final concentration: loaded with 1, 0.2, and 0.1 μg mL^{-1} Ce6). After incubation for 4 h, the wells were irradiated by laser for 5 min as described previously. Finally, the efficiency of biofilm eradication was evaluated *via* crystal violet staining and live/dead bacterial staining.

Furthermore, another model was built to confirm the biofilm inhibition ability of MPP-Ce6-mediated aPDT. Multispecies bacterial compounds (150 μL) and MPP-Ce6 (150 μL) were cocultured in a 48-well plate for 4 h. Then, the biofilm was irradiated with a 660-nm laser for 5 min at 0.5 W cm^{-2} per well. After treatment, the culture medium was exchanged with fresh BHI with 1% sucrose and continued to grow for another 20 h. On the second day and third day, two cycles of biofilm treatments were conducted as on the first day. At 72 h, the efficiency of biofilm inhibition was assessed using crystal violet staining, FE-SEM, and water-insoluble polysaccharide measurement.

FISH analysis: The successful construction of multispecies cariogenic biofilms was confirmed by FISH analysis. The biofilm was fixed in 4% paraformaldehyde for 20 min at RT. Subsequently, the biofilm was treated with Tris-EDTA buffer solution containing lysozyme (10 μg mL^{-1}) for 10 min at 37 °C. After dehydration by gradient concentrations of alcohol, specific oligonucleotide probes (Sangon Biotech Co., Ltd) were designed to label the various species of bacteria because of their specific 16S rRNA sequences. Finally, the biofilm on the cover glass was observed using CLSM. All processes were in the dark. The oligonucleotide probes aimed at different bacteria and their specific Ex/Em wavelengths are introduced in Table S2, Supporting Information.

Crystal violet staining: Crystal violet staining was used to quantify the amount of biofilm biomass. Specifically, the biofilms were first stained with 0.1% crystal violet solution for 15 min. After they were washed three times, 30% acetic acid was used to extract the dye for 10 min. Finally, the extraction was transferred into a 96-well plate, and the OD

values were read by a microplate reader at 660 nm (n = 3).

Live/dead bacterial staining: Live/dead bacterial staining was conducted according to the guidance of the Bacterial Viability Kit (LIVE/DEAD™ BacLight™, Invitrogen). Specifically, SYTO 9 (1.5 μL) and PI (1.5 μL) were diluted in saline (1 mL). Then, the mixture of SYTO 9 and PI at working concentrations was used to stain biofilms for 15 min in the dark. After they were rinsed three times and sealed with mounting medium, 3D images of biofilms were collected along the z-axis by CLSM (thickness of each layer: 0.5 μm). The Ex/Em wavelengths were 535/617 nm for PI and 485/498 nm for SYTO 9.

FE-SEM analysis: In this part, the sHA tablet (diameter, 9 mm; thickness, 2 mm) was used to mimic the pellicle-coated smooth tooth in the human oral cavity. After treatment with MPP-Ce6-mediated aPDT, the biofilms were washed and fixed with 4% glutaraldehyde at 4 °C for 4 h. Subsequently, the biofilms were dehydrated with 75%, 80%, 90%, 95%, and 100% alcohol successively. After critical-point drying in carbon dioxide, the samples were coated with gold and examined *via* FE-SEM (Sigma, Zeiss).

Water-insoluble polysaccharide measurement: An anthrone assay was used to quantify the water-insoluble polysaccharide [49]. Specifically, biofilms were first dissolved with NaOH solution (0.5 M), and then, ethanol was added to precipitate the polysaccharide. Afterwards, polysaccharides were collected *via* centrifugation and redissolved in NaOH solution (0.1 M). Then, the solution was slowly dropped into the anthrone solution (0.2% in sulfuric acid) and kept at 95 °C in a metal bath for 6 min. After it was recovered to RT, the OD values of the solution were measured using a microplate reader at 620 nm (n = 3).

Rat models of dental caries: All procedures concerning animal experiments were approved and under the supervision of the Institutional Animal Care and Use Committee of Wuhan University (S07920080A). Sprague−Dawley (SD) rats (15 days old) were used and fed in a specific-pathogen-free animal center of the Hospital of Stomatology, Wuhan University. First, to avoid the influence of endogenous oral microorganisms, 15-day-old SD rats were fed antibiotic water containing benzylpenicillin (200 μg mL^{-1}) and streptomycin sulfate (1500 μg mL^{-1}) as well as a diet supplemented with antibiotics (1 g kg^{-1}) for three consecutive days. The efficiency of antibiotic treatments was checked by plating onto MSB agar after swabbing the dental plaque in the oral cavity [44,50]. For the next three consecutive days, multispecies bacterial suspension (200 μL; 1 × 10^8 CFU mL^{-1}) was inoculated onto the tooth of each rat (twice a day) [51]. Afterwards, the efficiency of bacterial inoculation was checked as mentioned above [44,50]. Rats were fasted for 0.5 h before being swabbed and after bacterial inoculation. All rats were fed a cariogenic diet 2000 (Jiangsu Xietong Pharmaceutical Bioengineering CO., Ltd.) and 5% sucrose water from 18 days of age until the experiment finished.

Therapeutic schedules: Rats were randomly divided into five groups: MPP-Ce6+Laser, Free-Ce6+Laser, MPP-Ce6, Laser, and the Control group (eight rats per group). Treatments started when rats reached 21 days old. After they were anesthetized, MPP-Ce6 (loaded 20 μg mL^{-1} Ce6), Free-Ce6 (20 μg mL^{-1} Ce6) or PBS was applied to the teeth of the rats. Then, a 660-nm laser (0.5 W cm^{-2}, 3 min) was used to irradiate the three teeth on each side of the maxillary region. aPDT treatments were applied for three consecutive days and then continued to be performed every two days until the rats reached 47 days old. Both sides of the maxillary teeth were treated. No food or water was provided for at least 0.5 h after aPDT treatment. In addition, the Control and Laser groups were treated with PBS or laser alone, respectively. The weight and physical appearances of the rats from different groups were also recorded regularly.

Assessment of anti-caries efficiency in vivo: Sampling and CFU counting for cariogenic bacteria at different time points (23, 29, 35, 41, and 47 days old) were conducted as previously described [44,50]. After the rats were sacrificed by CO$_2$ asphyxiation at the end of treatment (47 days old), the jaws with teeth, oral mucosae, blood, and main organs were collected. The carious levels in the teeth were evaluated by micro-CT

and scored *via* Keyes' scoring method. H&E staining of the oral mucosa and main organs of rats was performed to evaluate the biocompatibility of different treatments. Blood biochemistry analysis was also conducted to measure liver and kidney function.

Statistical analysis: The results are presented as the mean ± standard deviation (SD). For the statistical analysis of CFU counting, data were log-transformed. All of the data were analyzed using GraphPad Prism. Ordinary one-way ANOVA was used when the data were normally distributed and variances were homogeneous. The Brown-Forsythe and Welch ANOVA was chosen when the data were normally distributed and variances were nonhomogeneous. The nonparametric Kruskal-Wallis was performed when the data were nonnormally distributed. Post hoc multiple comparisons were determined using Dunnett's test. $p < 0.05$ was set for statistical significance.

CRediT authorship contribution statement

Danfeng Liu: Conceptualization, Methodology, Formal analysis, Investigation, Data curation, Writing – original draft, Writing – review & editing, Visualization. **Xianbin Ma:** Conceptualization, Methodology, Formal analysis, Investigation, Data curation, Writing – review & editing, Visualization. **Yaoting Ji:** Writing – review & editing, Supervision, Project administration. **Rourong Chen:** Investigation. **Shuhui Zhou:** Investigation. **Hantao Yao:** Investigation. **Zichen Zhang:** Investigation. **Mengjie Ye:** Investigation. **Zhigang Xu:** Conceptualization, Resources, Writing – review & editing, Supervision, Project administration, Funding acquisition. **Minquan Du:** Conceptualization, Resources, Writing – review & editing, Supervision, Project administration, Funding acquisition.

Declaration of competing interest

The authors declare no conflict of interest.

Acknowledgements

Appendix A. Supplementary data

Supplementary data to this article can be found online at https://doi.org/10.1016/j.bioactmat.2021.12.016.

References

[1] N.B. Pitts, D.T. Zero, P.D. Marsh, K. Ekstrand, J.A. Weintraub, F. Ramos-Gomez, J. Tagami, S. Twetman, G. Tsakos, A. Ismail, Dental caries, Nat. Rev. Dis. Prim. 3 (2017) 17030.
[2] D.J. Manton, Child dental caries - a global problem of inequality, EClinicalMedicine 1 (2018) 3–4.
[3] R.H. Selwitz, A.I. Ismail, N.B. Pitts, Dental caries, Lancet 369 (2007) 51–59.
[4] I. Struzycka, The oral microbiome in dental caries, Pol. J. Microbiol. 63 (2014) 127–135.
[5] M. Astasov-Frauenhoffer, E.M. Kulik, Cariogenic biofilms and caries from birth to old age, Monogr. Oral Sci. 29 (2021) 53–64.
[6] A.F. Paes Leme, H. Koo, C.M. Bellato, G. Bedi, J.A. Cury, The role of sucrose in cariogenic dental biofilm formation–New insight, J. Dent. Res. 85 (2006) 878–887.
[7] W.H. Bowen, R.A. Burne, H. Wu, H. Koo, Oral biofilms: pathogens, matrix, and polymicrobial interactions in microenvironments, Trends Microbiol. 26 (2018) 229–242.
[8] B. Horev, M.I. Klein, G. Hwang, Y. Li, D. Kim, H. Koo, D.S. Benoit, Ph-activated nanoparticles for controlled topical delivery of farnesol to disrupt oral biofilm virulence, ACS Nano 9 (2015) 2390–2404.
[9] M. Kilian, I.L. Chapple, M. Hannig, P.D. Marsh, V. Meuric, A.M. Pedersen, M.S. Tonetti, W.G. Wade, E. Zaura, The oral microbiome - an update for oral healthcare professionals, Br. Dent. J. 221 (2016) 657–666.
[10] P.D. Marsh, Contemporary perspective on plaque control, Br. Dent. J. 212 (2012) 601–606.
[11] J.A. Aas, B.J. Paster, L.N. Stokes, I. Olsen, F.E. Dewhirst, Defining the normal bacterial flora of the oral cavity, J. Clin. Microbiol. 43 (2005) 5721–5732.
[12] K. Hojo, S. Nagaoka, T. Ohshima, N. Maeda, Bacterial interactions in dental biofilm development, J. Dent. Res. 88 (2009) 982–990.
[13] C.J. Seneviratne, C.F. Zhang, L.P. Samaranayake, Dental plaque biofilm in oral health and disease, Chin. J. Dent. Res. 14 (2011) 87–94.
[14] Y. Liu, Z. Ren, G. Hwang, H. Koo, Therapeutic strategies targeting cariogenic biofilm microenvironment, Adv. Dent. Res. 29 (2018) 86–92.
[15] M.S. Ibrahim, A.A. Balhaddad, I.M. Garcia, F.M. Collares, M.D. Weir, H.H.K. Xu, M.A.S. Melo, Ph-responsive calcium and phosphate-ion releasing antibacterial sealants on carious enamel lesions in vitro, J. Dent. 97 (2020) 103323.
[16] P.C. Naha, Y. Liu, G. Hwang, Y. Huang, S. Gubara, V. Jonnakuti, A. Simon-Soro, D. Kim, L. Gao, H. Koo, D.P. Cormode, Dextran-coated iron oxide nanoparticles as biomimetic catalysts for localized and Ph-activated biofilm disruption, ACS Nano 13 (2019) 4960–4971.
[17] Z. Zhao, C. Ding, Y. Wang, H. Tan, J. Li, Ph-responsive polymeric nanocarriers for efficient killing of cariogenic bacteria in biofilms, Biomater. Sci. 7 (2019) 1643–1651.
[18] M. Qi, M. Chi, X. Sun, X. Xie, M.D. Weir, T.W. Oates, Y. Zhou, L. Wang, Y. Bai, H.H. Xu, Novel nanomaterial-based antibacterial photodynamic therapies to combat oral bacterial biofilms and infectious diseases, Int. J. Nanomed. 14 (2019) 6937–6956.
[19] K. Konopka, T. Goslinski, Photodynamic therapy in dentistry, J. Dent. Res. 86 (2007) 694–707.
[20] M.R. Hamblin, Antimicrobial photodynamic inactivation: a bright new technique to kill resistant microbes, Curr. Opin. Microbiol. 33 (2016) 67–73.
[21] H. Zhang, Y.N. Zhu, Y. Li, X.Y. Qi, J. Yang, H.S. Qi, Q.S. Li, Y.M. Ma, Y. Zhang, X. Zhang, L. Zhang, A bifunctional Zwitterion-modified porphyrin for photodynamic nondestructive tooth whitening and biofilm eradication, Adv. Funct. Mater. 31 (2021) 2104799.
[22] Z. Li, W. Pan, E. Shi, L. Bai, H. Liu, C. Li, Y. Wang, J. Deng, Y. Wang, A multifunctional nanosystem based on bacterial cell-penetrating photosensitizer for fighting periodontitis via combining photodynamic and antibiotic therapies, ACS Biomater. Sci. Eng. 7 (2021) 772–786.
[23] Y.F. Ding, S. Li, L. Liang, Q. Huang, L. Yuwen, W. Yang, R. Wang, L.H. Wang, Highly biocompatible chlorin E6-loaded chitosan nanoparticles for improved photodynamic cancer therapy, ACS Appl. Mater. Interfaces 10 (2018) 9980–9987.
[24] D. Tichaczek-Goska, D. Wojnicz, K. Symonowicz, P. Ziolkowski, A.B. Hendrich, Photodynamic enhancement of the activity of antibiotics used in urinary tract infections, Laser Med. Sci. 34 (2019) 1547–1553.
[25] S. Liu, S. Qiao, L. Li, G. Qi, Y. Lin, Z. Qiao, H. Wang, C. Shao, Surface charge-conversion polymeric nanoparticles for photodynamic treatment of urinary tract bacterial infections, Nanotechnology 26 (2015) 495602.
[26] A. Shrestha, A. Kishen, Antibiofilm efficacy of photosensitizer-functionalized bioactive nanoparticles on multispecies biofilm, J. Endod. 40 (2014) 1604–1610.
[27] W. Li, E.S. Thian, M. Wang, Z. Wang, L. Ren, Surface design for antibacterial materials: from fundamentals to advanced strategies, Adv. Sci. 8 (2021) 2100368.
[28] P. Makvandi, U. Josic, M. Delfi, F. Pinelli, V. Jahed, E. Kaya, M. Ashrafizadeh, A. Zarepour, F. Rossi, A. Zarrabi, T. Agarwal, E.N. Zare, M. Ghomi, T. Kumar Maiti, L. Breschi, F.R. Tay, Drug delivery (Nano)Platforms for oral and dental applications: tissue regeneration, infection control, and cancer management, Adv. Sci. 8 (2021) 2004014.
[29] K.R. Sims, Y. Liu, G. Hwang, H.I. Jung, H. Koo, D.S.W. Benoit, Enhanced design and formulation of nanoparticles for anti-biofilm drug delivery, Nanoscale 11 (2018) 219–236.
[30] H. Takahashi, E.T. Nadres, K. Kuroda, Cationic amphiphilic polymers with antimicrobial activity for oral Care applications: eradication of S. Mutans biofilm, Biomacromolecules 18 (2017) 257–265.
[31] H. Deng, X. Li, Q. Peng, X. Wang, J. Chen, Y. Li, Monodisperse magnetic single-crystal ferrite microspheres, Angew Chem. Int. Ed. Engl. 44 (2005) 2782–2785.
[32] Z. Xu, P. Xue, Y.E. Gao, S. Liu, X. Shi, M. Hou, Y. Kang, Ph-responsive polymeric micelles based on poly(ethyleneglycol)-B-Poly(2-(Diisopropylamino) ethyl methacrylate) block copolymer for enhanced intracellular release of anticancer drugs, J. Colloid Interface Sci. 490 (2017) 511–519.
[33] X.L. Zhang, X.B. Ma, S.L. Huang, F.Q. Wen, The toxicity performance of ph-responsive doxorubicin nanocarrier with different drug loading strategy, Mater. Today Commun. 25 (2020) 101634.
[34] N. Takahashi, B. Nyvad, The role of bacteria in the caries process: ecological perspectives, J. Dent. Res. 90 (2011) 294–303.
[35] C. Wang, P. Chen, Y. Qiao, Y. Kang, Y. Yan, S. Guo, D. Wu, J. Wang, H. Wu, Bacteria-activated chlorin E6 ionic liquid based on cation and anion dual-mode antibacterial action for enhanced photodynamic efficacy, Biomater. Sci. 7 (2019) 1399–1410.
[36] P. Lingstrom, T. Imfeld, D. Birkhed, Comparison of three different methods for measurement of plaque-ph in humans after consumption of soft bread and potato chips, J. Dent. Res. 72 (1993) 865–870.

[37] D. Hu, Y. Deng, F. Jia, Q. Jin, J. Ji, Surface charge switchable supramolecular nanocarriers for nitric oxide synergistic photodynamic eradication of biofilms, ACS Nano 14 (2020) 347–359.

[38] Y. Wang, Y. Yang, Y. Shi, H. Song, C. Yu, Antibiotic-free antibacterial strategies enabled by nanomaterials: progress and perspectives, Adv. Mater. 32 (2020) 1904106.

[39] C. Yang, Y. Luo, H. Lin, M. Ge, J. Shi, X. Zhang, Niobium carbide mxene augmented medical implant elicits bacterial infection elimination and tissue regeneration, ACS Nano 15 (2021) 1086–1099.

[40] M.R. Hamblin, T. Hasan, Photodynamic therapy: a new antimicrobial approach to infectious disease? Photochem. Photobiol. Sci. 3 (2004) 436–450.

[41] I. Suzuki, T. Shimizu, H. Senpuku, Short chain fatty acids induced the type 1 and type 2 Fimbrillin-dependent and Fimbrillin-independent initial attachment and colonization of actinomyces oris monoculture but not coculture with streptococci, BMC Microbiol. 20 (2020) 329.

[42] B. Lindquist, C.G. Emilson, Dental location of Streptococcus mutans and Streptococcus sobrinus in humans Harboring both species, Caries Res. 25 (1991) 146–152.

[43] C.V. Pereira, L.J. Pereira, R.B. Goncalves, J.F. Hofling, In vitro bacterial plaque suppression and recolonization by S-mutans and S-sobrinus, Braz. J. Microbiol. 37 (2006) 20–25.

[44] Q. Zhang, S. Qin, X. Xu, J. Zhao, H. Zhang, Z. Liu, W. Chen, Inhibitory effect of lactobacillus plantarum Ccfm8724 towards Streptococcus mutans- and Candida albicans-induced caries in rats, Oxid. Med. Cell. Longev. 2020 (2020) 4345804.

[45] P.H. Keyes, Dental caries in the molar teeth of rats. I. Distribution of lesions induced by high-carbohydrate low-fat diets, J. Dent. Res. 37 (1958) 1077–1087.

[46] P.H. Keyes, Dental caries in the molar teeth of rats. Ii. A method for diagnosing and scoring several types of lesions simultaneously, J. Dent. Res. 37 (1958) 1088–1099.

[47] M.V. Swain, J. Xue, State of the art of micro-ct applications in dental research, Int. J. Oral Sci. 1 (2009) 177–188.

[48] L.L. Yang, L. Zhang, S.C. Wan, S. Wang, Z.Z. Wu, Q.C. Yang, Y. Xiao, H.X. Deng, Z. J. Sun, Two-photon absorption induced cancer immunotherapy using covalent organic frameworks, Adv. Funct. Mater. 31 (2021) 2103056.

[49] H. Koo, M.F. Hayacibara, B.D. Schobel, J.A. Cury, P.L. Rosalen, Y.K. Park, A. M. Vacca-Smith, W.H. Bowen, Inhibition of Streptococcus mutans biofilm accumulation and polysaccharide production by apigenin and Tt-Farnesol, J. Antimicrob. Chemother. 52 (2003) 782–789.

[50] K. Takada, K. Hayashi, K. Sasaki, T. Sato, M. Hirasawa, Selectivity of mitis salivarius agar and a new selective medium for oral streptococci in dogs, J. Microbiol. Methods 66 (2006) 460–465.

[51] S. Beiraghi, S. Rosen, F. Beck, The effect of stannous and sodium fluoride on coronal caries, root caries and bone loss in rice rats, Arch. Oral Biol. 35 (1990) 79–80.